Deep learning approach for inverse design of metasurfaces with a wider shape gamut

Article *in* Optics Letters · May 2022

DOI: 10.1364/OL.458746

Soumyashree Soumyaprakash Panda
Indian Institute of Technology Gandhinagar

Sumit Choudhary
Indian Institute of Technology Mandi

Satinder K. Sharma
Indian Institute of Technology Mandi MANDI (Himachal Pradesh) India

Ravi Sadananda Hegde
Indian Institute of Technology Gandhinagar

Optics Letters

Deep learning approach for inverse design of metasurfaces with a wider shape gamut

Soumyashree S. Panda,[1] Sumit Choudhary,[2] Siddharth Joshi,[1] Satinder K. Sharma,[2] and Ravi S. Hegde[1,*]

[1] Electrical Engineering Discipline, Indian Institute of Technology, Gandhinagar, 382355, India
[2] School of Computing and Electrical Engineering, Indian Institute of Technology, Mandi, 175005, India
*Corresponding author: hegder@iitgn.ac.in

Received 17 March 2022; revised 21 April 2022; accepted 28 April 2022; posted 28 April 2022; published 13 May 2022

While the large design degrees of freedom (DOFs) give metasurfaces a tremendous versatility, they make the inverse design challenging. Metasurface designers mostly rely on simple shapes and ordered placements, which restricts the achievable performance. We report a deep learning based inverse design flow that enables a fuller exploitation of the meta-atom shape. Using a polygonal shape encoding that covers a broad gamut of lithographically realizable resonators, we demonstrate the inverse design of color filters in an amorphous silicon material platform. The inverse-designed transmission-mode color filter metasurfaces are experimentally realized and exhibit enhancement in the color gamut.

https://doi.org/10.1364/OL.458746

Optical metasurfaces enable exquisite control over an incident wavefront's properties and are being actively explored for diverse applications in imaging, sensing, holography, and optical computing. In its most general form, the optical metasurface is a "surface-like" heterogeneous array of nanoresonators. Despite their promise, metasurface designs reported in the literature are still predominantly limited to ordered arrangements of primitive geometries; e.g., circular [3], elliptical [4], rectangular [5], and cross-shaped nanopillars [6]. Inverse designs using limited degrees of freedom (DOFs) is considerably simple, but may exhibit suboptimal optical performance in comparison to that obtainable with the entire universe of lithographically realizable designs. The metasurface design repertoire is slowly expanding to include complex geometries like polygonal meta-atoms [7–9], free-form geometries [10–14], extended meta-atoms [15], and volumetric structures [16]. Typically, inverse design involving complex geometries uses topology optimization or metaheuristic optimization algorithms (like genetic algorithm, swarm optimization, differential evolution etc. [17,18]). However, the workflow for such inverse design, especially the geometry parameterization step, is non-trivial. If not carefully chosen, a parameterization could vastly enlarge the design space without ensuring that most of the shapes remain realizable. The optical response of complex shape sets is non-intuitive and enlarged search spaces complicate the optimization process.

Artificial intelligence (AI) and related data-driven techniques [19–22] are being increasingly explored for inverse design problems in nanophotonics. Current approaches for shape encoding can be divided into three broad categories: (1) parametric representation [23]; (2) pixelated image representation [24–26]; and 3) generative networks and learned latent space representations [27–29]. Approach 1 is the simplest but results in a very restricted shape set. Approach 2, however, results in a large space set, but a large fraction of this set is unfeasible resulting in a highly inefficient model creation. Zandehshahvar *et al.* [29] implemented auto-encoders in generative adversarial networks (GAN) to map the design performance to a latent space for manifold learning; but consider a limited number of design classes. Lin *et al.* [30] used variational autoencoders in a GAN to design geometries with predefined symmetries; however, coaching the generative network to restrict itself to lithographically feasible shapes remains a challenge. Wen and co-workers [28] proposed "self-attention layers" in the progressive growth of GAN (PGGAN) for design robustness. Chen *et al.* [31] proposed a design under uncertainty framework in addition to a GAN that takes fabrication uncertainty into account. However, these methods result in complicated workflows as they require training additional networks. Furthermore, adversarial training of generative networks is known to exhibit problems like loss oscillations.

In this work, we consider a polygonal shape encoding [8], a parametric representation of meta-atom geometry (approach 1), which broadens the shape gamut and enables the training of a high-accuracy predictive model without requiring a large training dataset. We show that such a predictive model can be used as a surrogate fitness evaluator for an evolutionary optimizer resulting in significant reduction in optimization time without compromising on solution quality. To demonstrate the utility of our proposed design method, we consider an inverse design of transmission-mode metasurface color filter arrays (CFA) [32] in an amorphous silicon (a-Si) platform. The inverse-designed structures are fabricated and performance improvements are demonstrated experimentally.

We consider a periodic 100-nm-thick a-Si metasurface on a silica substrate [see Fig. 1(a)] with a single polygon-shaped nanoresonator in each unit cell. The polygons are encoded (see Section S-1 in Supplement 1) via the polar coordinates of its

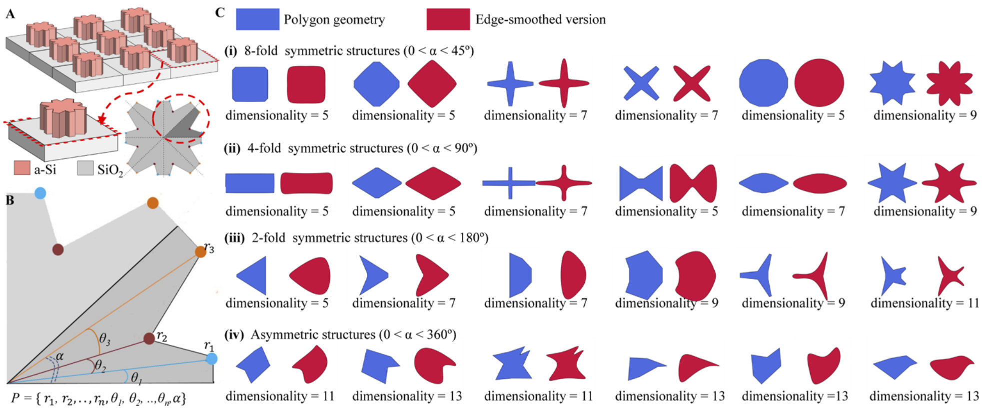

Fig. 1. Encoding a gamut of lithographically realizable nanoresonator shapes. (a) Periodic metasurface with 8-fold symmetric free-form nanoresonators. Inset: top view of a unit cell. (b) Expanded view of one octant of the 8-fold symmetric polygon with the vertices labeled with corresponding r and θ. Highest value of angle (α) is marked with a dashed arc (see Section S-1 in Supplement 1). (c) Plethora of geometries (symmetric and asymmetric) possible with the proposed polygonal encoding beginning with polygon definition and boundary smoothing. Dimensionality of the parameter vector [shown in panel (b)] required to define the shape is specified for each example.

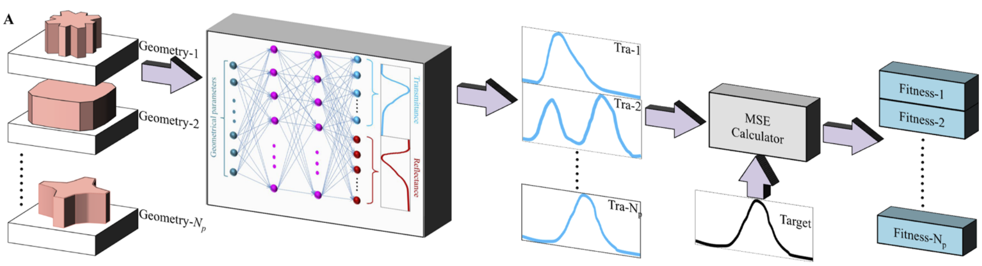

Fig. 2. Trained neural network used as a surrogate fitness estimator (see Fig. S1 in Supplement 1 for details).

vertices: radius (r) and angle weight (ϕ) and highest angle (α) [Fig. 1(b)]. As seen in Fig. 1(c), this encoding can encompass a wide gamut of shapes. We focus on polarization independent metasurface color filters by imposing an 8-fold symmetry. The number of points per octant is fixed to 3; giving us a 7-dimensional parameter vector, which will be the "input" to our deep neural network (DNN) surrogate model. The transmittance and reflectance spectra at 32 wavelengths, with measurements taken 10 nm apart in the visible wavelength range (400–710 nm), constitute the "output" of the DNN model. Extensive details regarding the ground truth generation, DNN training, and validation, as well as their timing along with DNN prediction results for higher dimensional geometries, are provided in Section S-2 in Supplement 1.

The next phase concerns the use of such trained DNNs as a surrogate fitness estimator (Fig. 2) in an evolutionary optimization [8,9]. Specifically, we use multi-island differential evolution (DE) as the evolutionary algorithm (see full details in Section S-3 in Supplement 1). For comparison purposes, we also used the full simulator for fitness evaluation. Henceforth, the normal and surrogate DE optimizations are referred to as DE_S^4 and DE_NN, respectively. As the interest is in designing color filters, the color matching functions of expected colors (RGB or CMY) are taken as target spectra and fitness values are assigned to the polygon metasurface structures on the basis of how close the predicted spectra are to the target.

For a typical DE optimization [8] with fixed number of islands (3) and population size (70), the time taken for DE_S^4 and DE_NN are ~72 minutes and 100 seconds, respectively. For robust DE optimization [9] with the same number of islands (3) and population size (70), DE_S^4 and DE_NN take ~18.5 hours and 155 seconds, respectively. This shows a radical advantage of DE_NN over DE_S^4 and will be especially useful when the surrogate creation cost can be amortized across multiple optimizations. First, despite being significantly faster, optimizations relying on surrogate fitness evaluation do not reach suboptimal designs as seen by comparing DE_S^4 and DE_NN [Figs. 3(a) and 3(b)]. Direct and surrogate optimizations are observed to both result in nearly identical designs with closely matching optical response and perceptually similar coloration. This claim is further reinforced by comparing direct and surrogate optimization results for attaining various target functionalities, as given in Fig. S-2 of the supporting document.

Lastly, the metasurface color filters optimized with DE_NN were fabricated and experimentally characterized (see Fig. S-4 and Fig. S-5 of the supporting document for fabrication process and experimental results in Supplement 1). The unit cell geometries of fabricated structures (extracted with SEM micrography) are compared with the theoretical designs for RGB and CMY color filters in Figs. 4(a) and 4(b), respectively. Roughly 40 μm×40 μm patches of color filters (120×120 arrays of the unit cells) were fabricated and the optical characterization of the color filters was performed. The transmitted experimental colors are compared with expected simulated colors in all of the RGB and CMY color filters and a great deal of similarity can be observed between them. The experimental colors were picked from the optical characterization images and the chromaticity coordinates were calculated; shown in Fig. 4(c). In RGB color

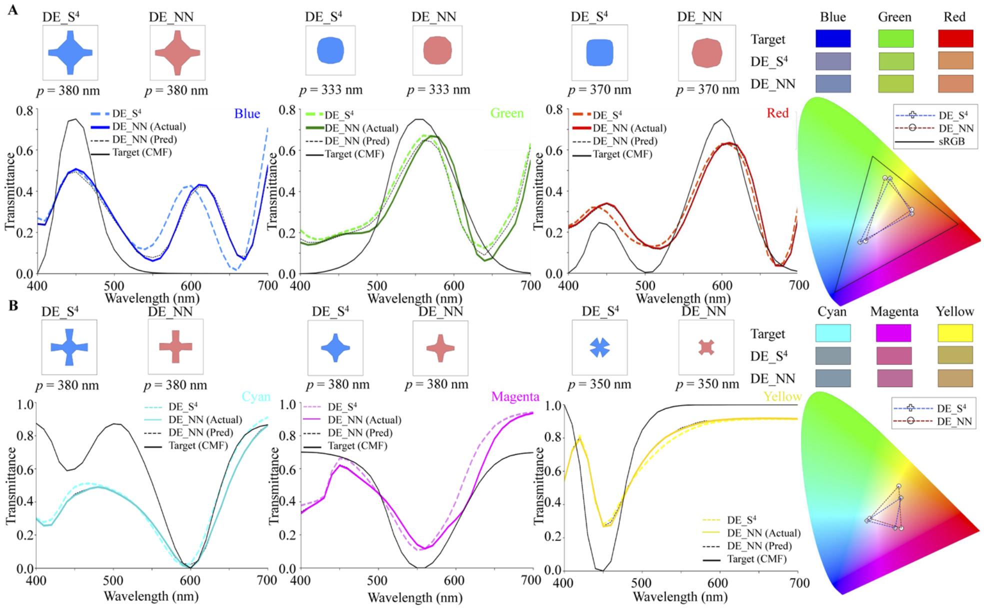

Fig. 3. Surrogate optimization of transmission-mode polygon-shaped metasurface RGB and CMY color filter arrays. (a),(b) Comparison of the final optimal designs and their spectra obtained by DE_S[4] and DE_NN. Corresponding CMFs are shown for reference. For surrogate optimization both the DNN predicted spectra and that obtained by RCWA simulation are shown. Obtained colors are plotted in the CIE 1931 chromaticity diagram along with the corresponding color patches.

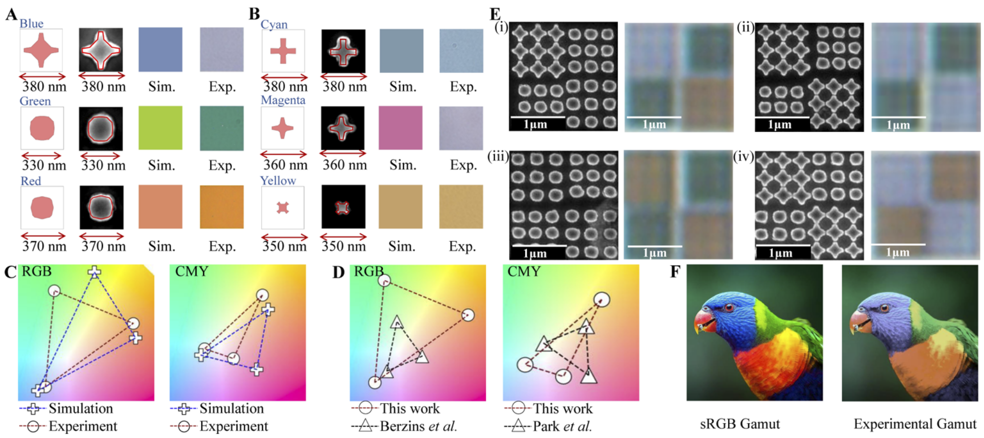

Fig. 4. Experimental results of polygon-shaped RGB and CMY color filters optimized by DE_NN. (a),(b) SEM images of fabricated color filter unit cell geometries are compared with respective theoretical designs. The theoretical (obtained with simulation) and experimental colors (obtained through optical characterization) are also compared. (c) Comparison of simulated and experimental color gamuts. (d) Comparison of experimental color gamuts with the gamuts reported in Refs. [1,2]. (e) Arrangement of 1 μm × 1 μm RGB color filters in Bayer's patterns and checkerboard patterns. (SEM shown for reference.) (f) Comparison of an example image with colors limited to sRGB and experimental RGB color space.

filters, for blue and red colors, the chromaticity coordinates of fabricated and simulated colors are observed to lie in close proximity; whereas the green color is observed to have a decreased luminescence. In CMY color filters, similarity can be observed between the simulated and experimental colors for cyan and yellow filters; but magenta is observed near the gray point in experimental design.

Color gamuts of cylindrical color filters built on the same material platform for RGB [1] and CMY [2] color filters are compared with the experimental gamut in Fig. 4(d). The experimental color gamuts for this work are observed to show an improvement; providing the efficacy of polygonal geometries.

The optical and SEM micrography of RGB color filters arranged in 1 μm×1 μm Bayer's patterns and checkerboard (BG, GR, BR) patterns are provided in Fig. 4(e). It is observed that color purity of the experimental filters hold true for a filter size as small as 1 μm. Figure 4(f) shows an example image when its colors are limited between the sRGB color space and the experimental color space to show the extent of color purity obtained by the designed polygonal color filters.

This work can be extended by considering optical characteristics like incident-angle and polarization dependence. The design turnaround time can be further improved by smart-sampling strategies that reduce the burden of ground-truth generation

[15]. In our previous works [33,34], we have explored surrogate-assisted optimization in cases where the learned model has low accuracy and found that using a combination of exact and surrogate based approximate fitness evaluations can be used to trade-off between optimality and computation budget.

Funding. Nano Mission Council (SN/NM/NS-65/2016); Indian Institute of Technology.

Acknowledgement. We acknowledge Department of Science and Technology, India Nanomission Project: SN/NM/NS-65/2016 and the Centre for Design and Fabrication of Electronic Devices (C4DFED), Indian Institute of Technology, Mandi, India.

Disclosures. The authors declare no conflicts of interest.

Data availability. The source code for the implementation, datasets and saved models can be found in Ref. [35].

Supplemental document. See Supplement 1 for supporting content.

REFERENCES

1. J. Berzins, S. Fasold, T. Pertsch, S. M. Baumer, and F. Setzpfandt, ACS Photonics **6**, 1018 (2019).
2. C.-S. Park, V. R. Shrestha, W. Yue, S. Gao, S.-S. Lee, E.-S. Kim, and D.-Y. Choi, Sci. Rep. **7**, 2556 (2017).
3. Y. Horie, S. Han, J.-Y. Lee, J. Kim, Y. Kim, A. Arbabi, C. Shin, L. Shi, E. Arbabi, S. M. Kamali, H.-S. Lee, S. Hwang, and A. Faraon, Nano Lett. **17**, 3159 (2017).
4. J. Jin, J. Luo, X. Zhang, H. Gao, X. Li, M. Pu, P. Gao, Z. Zhao, and X. Luo, Sci. Rep. **6**, 24286 (2016).
5. C. Damgaard-Carstensen, F. Ding, C. Meng, and S. I. Bozhevolnyi, Sci. Rep. **10**, 19031 (2020).
6. V. Vashistha, G. Vaidya, R. S. Hegde, A. E. Serebryannikov, N. Bonod, and M. Krawczyk, ACS Photonics **4**, 1076 (2017).
7. S. Inampudi and H. Mosallaei, Appl. Phys. Lett. **112**, 241102 (2018).
8. S. S. Panda and R. S. Hegde, J. Nanophoton. **14**, 016014 (2020).
9. S. S. Panda, H. S. Vyas, and R. S. Hegde, Opt. Mater. Express **10**, 3145 (2020).
10. J. Andkjaer, V. E. Johansen, K. S. Friis, and O. Sigmund, J. Opt. Soc. Am. B **31**, 164 (2014).
11. D. Sell, J. Yang, S. Doshay, R. Yang, and J. A. Fan, Nano Lett. **17**, 3752 (2017).
12. Z. Shi, A. Y. Zhu, Z. Li, Y.-W. Huang, W. T. Chen, C.-W. Qiu, and F. Capasso, Sci. Adv. **6**, eaba3367 (2020).
13. J. Trisno, H. Wang, H. T. Wang, R. J. Ng, S. Daqiqeh Rezaei, and J. K. Yang, Adv. Photo. Res. **1**, 2000068 (2020).
14. J. Jiang, D. Sell, S. Hoyer, J. Hickey, J. Yang, and J. A. Fan, ACS Nano **13**, 8872 (2019).
15. S. S. Panda and R. S. Hegde, Nanophotonics **11**, 345 (2022).
16. P. Camayd-Muñoz, C. Ballew, G. Roberts, and A. Faraon, Optica **7**, 280 (2020).
17. S. D. Campbell, D. Sell, R. P. Jenkins, E. B. Whiting, J. A. Fan, and D. H. Werner, Opt. Mater. Express **9**, 1842 (2019).
18. J. Park, S. Kim, D. W. Nam, H. Chung, C. Y. Park, and M. S. Jang, Nanophotonics **11**, 1809 (2022).
19. W. Ma, Z. Liu, Z. A. Kudyshev, A. Boltasseva, W. Cai, and Y. Liu, Nat. Photonics **15**, 77 (2021).
20. R. S. Hegde, Nanoscale Adv. **2**, 1007 (2020).
21. O. Khatib, S. Ren, J. Malof, and W. J. Padilla, Adv. Funct. Mater. **31**, 2101748 (2021).
22. S. So, T. Badloe, J. Noh, J. Bravo-Abad, and J. Rho, Nanophotonics **9**, 1041 (2020).
23. C. C. Nadell, B. Huang, J. M. Malof, and W. J. Padilla, Opt. Express **27**, 27523 (2019).
24. J. S. Jensen and O. Sigmund, Laser Photonics Rev. **5**, 308 (2011).
25. S. Jafar-Zanjani, S. Inampudi, and H. Mosallaei, Sci. Rep. **8**, 11040 (2018).
26. T. Zhang, Y. S. Ang, E. Li, C. Y. Kee, and L. Ang, “SUTD-PRCM dataset and neural architecture search approach for complex metasurface design,” arXiv:2203.00002 (2022).
27. Z. Liu, D. Zhu, S. P. Rodrigues, K.-T. Lee, and W. Cai, Nano Lett. **18**, 6570 (2018).
28. F. Wen, J. Jiang, and J. A. Fan, ACS Photonics **7**, 2098 (2020).
29. M. Zandehshahvar, Y. Kiarashinejad, M. Zhu, H. Maleki, T. Brown, and A. Adibi, ACS Photonics **9**, 714 (2022).
30. R. Lin, Z. Alnakhli, and X. Li, Photonics. Res. **9**, B96 (2021).
31. W. W. Chen, D. Lee, and W. Chen, “Deep generative models for geometric design under uncertainty,” arXiv:2112.08919 (2021).
32. F. Gildas and Y. Dan, J. Nanophoton. **13**, 020901 (2019).
33. R. Hegde, OSA Continuum **4**, 1019 (2021).
34. R. S. Hegde, IEEE J. Select. Topics Quantum Electron. **26**, 7700908 (2020).
35. Soumyashree S. Panda, “A deep learning approach for inverse design of metasurfaces with a wider shape gamut,” GitHub (2022), https://github.com/soumyashree-panda/metasurface-knowledge-discovery